Earth and Planetary Science Letters 380 (2013) 21–30

Contents lists available at ScienceDirect

Earth and Planetary Science Letters

www.elsevier.com/locate/epsl

Does calving matter? Evidence for significant submarine melt

Timothy C. Bartholomaus [a,b,*], Christopher F. Larsen [a], Shad O'Neel [c,b]

[a] Geophysical Institute, University of Alaska Fairbanks, 903 Koyukuk Dr., Fairbanks, AK 99775, USA
[b] Dept. of Geology and Geophysics, University of Alaska Fairbanks, 900 Yukon Dr., Fairbanks, AK 99775, USA
[c] Alaska Science Center, U.S. Geological Survey, 4210 University Dr., Anchorage, AK 99508, USA

ARTICLE INFO

Article history:
Received 20 February 2013
Received in revised form 9 July 2013
Accepted 6 August 2013
Available online xxxx
Editor: J. Lynch-Stieglitz

Keywords:
tidewater glacier
submarine melt
iceberg calving
glacier dynamics
fjord circulation

ABSTRACT

During the summer in the northeast Pacific Ocean, the Alaska Coastal Current sweeps water with temperatures in excess of 12 °C past the mouths of glacierized fjords and bays. The extent to which these warm waters affect the mass balance of Alaskan tidewater glaciers is uncertain. Here we report hydrographic measurements made within Icy Bay, Alaska, and calculate rates of submarine melt at Yahtse Glacier, a tidewater glacier terminating in Icy Bay. We find strongly stratified water properties consistent with estuarine circulation and evidence that warm Gulf of Alaska water reaches the head of 40 km-long Icy Bay, largely unaltered. A 10–20 m layer of cold, fresh, glacially-modified water overlies warm, saline water. The saline water is observed to reach up to 10.4 °C within 1.5 km of the terminus of Yahtse Glacier. By quantifying the heat and salt deficit within the glacially-modified water, we place bounds on the rate of submarine melt. The submarine melt rate is estimated at >9 m d^{-1}, at least half the rate at which ice flows into the terminus region, and can plausibly account for all of the submarine terminus mass loss. Our measurements suggest that summer and fall subaerial calving is a direct response to thermal undercutting of the terminus, further demonstrating the critical role of the ocean in modulating tidewater glacier dynamics.

1. Introduction

Marine-terminating glaciers worldwide are undergoing rapid changes (e.g., Larsen et al., 2007; Pritchard et al., 2009). In many cases, rapid mass changes of tidewater glaciers are controlled by processes acting at the terminus (Nick et al., 2009). Changes in glacier terminus position dL/dt result from differences in the ice flux to the terminus Q_i and ice flux from the terminus,

$$\frac{dL}{dt} = \frac{Q_i - Q_a}{A} \tag{1}$$

where Q_a is the frontal ablation rate (i.e., rate of ice loss from the glacier terminus, Cogley et al., 2011), and A is the cross-sectional area of the terminus. The terminus ice flux $Q_i = u_i A$, where u_i is the terminus-averaged ice velocity. Ice melt (both above and below the water line) and iceberg calving contribute to the frontal ablation rate. In accordance with previous studies in Alaska that found submarine melt rates 100-fold greater than subaerial melt rates (Walters et al., 1988; Motyka et al., 2003), we disregard subaerial frontal melt. The flux of ice lost to submarine melt Q_m is

$$Q_m = \dot{m} A_w, \tag{2}$$

where $\dot{m}$ is the terminus-averaged submarine melt rate, and A_w is the submarine portion of the terminus cross-section A, and similarly, the calving flux Q_c is

$$Q_c = \dot{c} A, \tag{3}$$

where $\dot{c}$ is the terminus-averaged calving rate. Grounded tidewater glaciers are unable to support significantly overhanging termini (O'Leary and Christoffersen, 2013), so, in essence,

$$dL/dt = u_i - \dot{c} - \dot{m}, \tag{4}$$

and where $dL/dt \ll u_i$, as is frequently the case (van der Veen, 2002),

$$u_i \sim \dot{c} + \dot{m}. \tag{5}$$

While, in many tidewater systems, the components of Eq. (4) are clearly changing, the calving and submarine melt processes are poorly understood and their rates are difficult to measure. Quantifying the magnitude of the submarine melt rate, and therefore the relative size of $\dot{m}$ and $\dot{c}$, at Yahtse Glacier, Alaska, is the goal of this study.

* Corresponding author at: Geophysical Institute, University of Alaska Fairbanks, 903 Koyukuk Dr., Fairbanks, AK 99775, USA.
E-mail address: tbartholomaus@gi.alaska.edu (T.C. Bartholomaus).

0012-821X/$ – see front matter
http://dx.doi.org/10.1016/j.epsl.2013.08.014

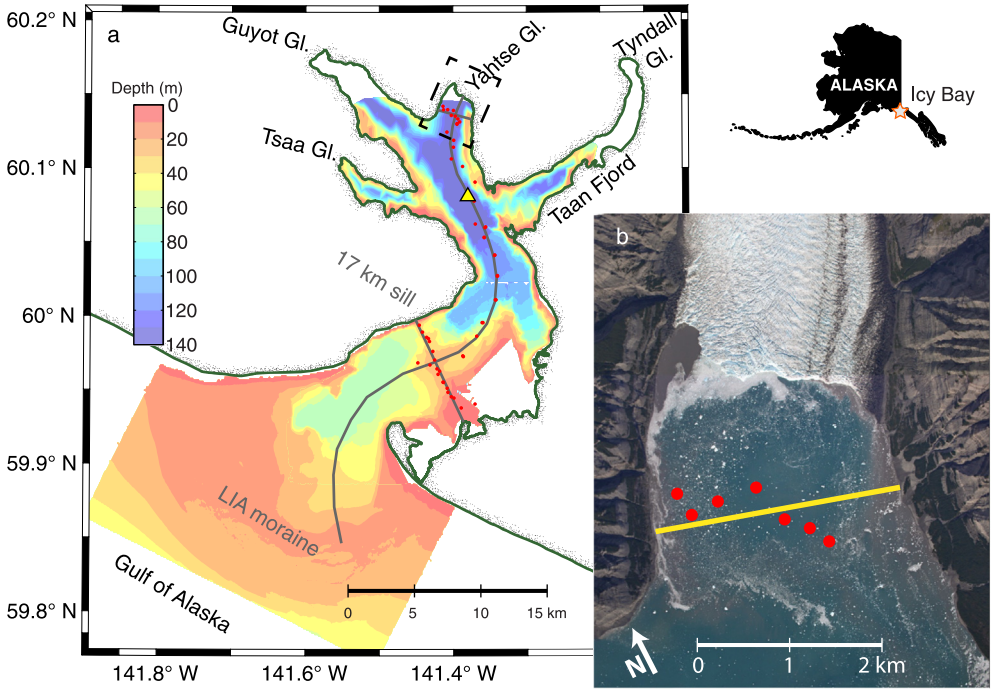

Fig. 1. Map of the study area. (a) Icy Bay with 10 m bathymetric filled contours. The shoreline is identified in green and two shallow sills are labeled. The locations of CTD casts made in 2011 are shown as small red circles. The locations of cross-section profiles (Fig. 3 and supplemental material) are shown in gray. The 2011 termini of four glaciers are identified. The area of panel (b) is enclosed within the dashed black rectangle. The location of the casts presented in Fig. 2 is marked with a yellow triangle. (b) Aerial photograph of the terminus of Yahtse Glacier (12 Sept. 2011), the locations of the 7 CTD casts presented in Figs. 3 and 4 (29 July 2011), and the fjord-perpendicular profile onto which these casts are projected. The persistent subglacial discharge plume is apparent on the NW side of the terminus. During late July 2011, it extended to include the location of the 2 western-most casts. (For interpretation of the references to color in this figure legend, the reader is referred to the web version of this article.)

Theoretical and modeling studies have found that the submarine melt rate at a glacier terminus is dependent on subglacial discharge and ambient seawater temperature, such that

$$\dot{m} \propto q^p \Theta_s, \tag{6}$$

where q is the flux of subglacial discharge per terminus length, p is a parameter, and Θ_s is the ambient seawater temperature (Jenkins, 2011; Xu et al., 2012; Sciascia et al., 2013). Both Jenkins (2011) and Xu et al. (2012) found $p = 1/3$, whereas $p = 1/2$ better fit the modeling results of Sciascia et al. (2013).

Several authors have attributed rapid geometry changes observed at tidewater glacier termini in Alaska and Greenland to submarine melt (e.g., Motyka et al., 2003; Ritchie et al., 2008; Nick et al., 2009; Seale et al., 2011). In Alaska, several studies have demonstrated that warm (>7 °C) water can reach within 2–3 km of tidewater glacier termini (Matthews, 1981; Walters et al., 1988; Motyka et al., 2003). Submarine melt rates across Alaska are poorly resolved, but have been shown to reach up to 12 m d^{-1} averaged across submarine termini (Walters et al., 1988; Motyka et al., 2003). However, despite these observations, substantial uncertainty persists regarding the temporal and spatial extent over which submarine ice melt is important, the upper bound of $\dot{m}$, and the interplay within glacierized fjords between subglacial discharge, submarine melt, and continental shelf seawater.

Herein, we present observations and model results of submarine melt at Yahtse Glacier and Icy Bay, located along the Gulf of Alaska coast, based upon 123 conductivity–temperature–depth (CTD) casts made during Julys in 2009–2011. These hydrographic measurements reveal a 10–20 m thick, surface layer of glacially-modified water and allow us to infer the near-terminus fjord circulation. Adjacent to the terminus of Yahtse Glacier, we draw on observations of water temperature and salinity to identify the amount of submarine glacier melt, subglacial discharge and ambient seawater present within the glacially-modified water. To quantify the flux of these waters, and therefore $\dot{m}$, we estimate the near-surface currents with a variety of local observations. Finally, we place our summer-time estimate into longer, seasonal, annual and multi-decadal contexts.

2. Field site

Ice Bay is a 40-km-long indentation on the Gulf of Alaska coast (Fig. 1). During the summer, the Alaska Coastal Current (ACC) sweeps warm (>12 °C) near-surface water north and west along Alaska's continental shelf, past the mouth of Icy Bay (Stabeno et al., 2004; Weingartner et al., 2005). This baroclinic current is driven in large part by fresh water delivery along the coast. Since much of this fresh water is glacier runoff (Neal et al., 2010), the influence of glaciers on the current is unquestioned (Weingartner et al., 2005; Royer and Grosch, 2006). However, the reciprocal relationship, the current's influence on glaciers, is poorly understood despite the current's potential to impose a significant melt forcing on the termini of all tidewater glaciers surrounding the Gulf of Alaska.

Icy Bay was entirely occupied by glaciers flowing out of the St. Elias Range during the mid-19th century (Fig. 1) (Porter, 1989; Barclay et al., 2006). Near the end of the 19th century, the coalesced tidewater Icy Bay glaciers began a 100 yr retreat from their Little Ice Age (LIA) maximum at an average rate of 400 m yr^{-1}. This retreat culminated in the division of the Icy Bay glaciers into several distinct, formerly tributary glaciers, of which Yahtse Glacier has the largest area (1020 km^2 in 2000). Yahtse Glacier reached its most-retracted position in approximately 1990, after which it began a 2 km re-advance that continues today. Since 2009, we have observed a spring advance and fall retreat (approximately 300 m range) superimposed on the multi-year advance (Bartholomaus et al., 2012).

Icy Bay is separated from the Gulf of Alaska by a submarine terminal moraine at the location of the LIA maximum; the maximum depth across the crest of this moraine/sill is 17 m.

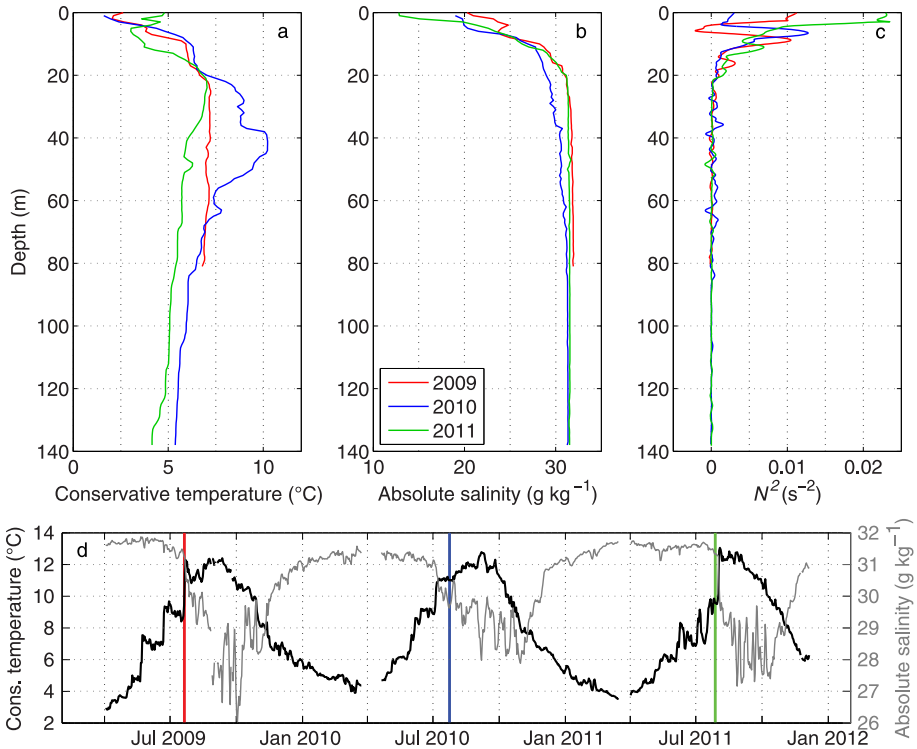

Fig. 2. Three years of hydrographic data. (a)–(c) Representative late-July casts from 3 consecutive years at a location between Tsaa and Taan fjords, 33 km from the LIA maximum and 8 km from the Yahtse terminus. (d) Daily-averaged, 20-m-depth conservative temperature and absolute salinity at station GAK1, a location within the ACC 450 km west of Icy Bay. Vertical, colored lines identify the times of each of the three casts in panels (a)–(c).

The continental shelf extends for 60 km off-shore. Inland by 17 km of the LIA maximum sill is a second, intermediate sill with a maximum depth of 35 m. The retreat of the Icy Bay glaciers paused here between 1916 and 1926 (Porter, 1989). In 1981, as Yahtse Glacier was approaching its most receded position, the greatest depths within Icy Bay (∼185 m) were found within the narrow Yahtse Glacier fjord (Post, 1983). Most of the bathymetry in Fig. 1a was collected between 2000 and 2008 by the U.S. National Oceanic and Atmospheric Administration (NOAA) (www.ngdc.noaa.gov/mgg/bathymetry/relief.html). Near the glacier termini, where multibeam data are unavailable, we contour the 1981 soundings (Post, 1983, and NOAA Icy Bay nautical chart 16741). Soundings reported in this study reveal shallowing by more than 50 m near the Yahtse Glacier terminus; thus, we have low confidence in these near-terminus depths (Section 4).

Tides have been recorded within 3 km of the mouth of Taan Fjord. There, the difference between Mean Higher High Water and Mean Lower Low Water is 2.9 m (http://tidesandcurrents.noaa.gov, Tidal station 9453431).

3. Data collection and processing

During late July of 2009, 2010 and 2011, we made respectively 6, 55 and 62 CTD casts to characterize the hydrography within Icy Bay. Each year, we collected data with a Sea-Bird Electronics (SBE) 19 profiler. In 2011, an SBE 19 plus additionally recorded turbidity, pH, and dissolved oxygen. The manufacturer-provided accuracies for these instruments are $<0.01\,^{\circ}$C, <0.01 g kg^{-1}, and <1.7 dbar. Instruments were calibrated prior to use each year. Casts were made along three profiles: one profile along the axis of Icy Bay and two perpendicular transects (Fig. 1). The 2011 casts provide the best spatial coverage of Icy Bay and are the focus of this study. For plotting and analysis, water properties from each cast are averaged at 1 m intervals. To construct cross-sections of water properties, we project casts onto the profiles by translating them up to 0.5 km and linearly interpolating between measurements.

We place our CTD casts within a broader geographic and temporal context by drawing on measurements from GAK1, an oceanographic station within the ACC, 450 km west of Icy Bay (Weingartner et al., 2005). In particular, we choose to use water properties collected at 20 m depth, the shallowest moored measurements. Other depths reveal water property variations with similar temporal structure to those at 20 m depth. For all analyses, we present water properties as conservative temperatures Θ and absolute salinities S_A, in accordance with the International Thermodynamic Equation of Seawater – 2010 (TEOS-10) (IOC et al., 2010).

A time lapse camera looking south above Icy Bay allows us to characterize near-surface water currents by the influence they exert on icebergs, as well as the rates of ice flow near the terminus. For 11 days during time lapse camera operation, we used an autotheodolite to survey the position of prisms placed on a serac 1 km from the glacier terminus. We extend this surveyed record of daily glacier speeds by cross-correlating time lapse images (following Scambos et al., 1992) and extracting the pixel offsets for the region where the prisms were placed. Linear regression of surveyed speed onto pixel offset enables us to identify glacier terminus speeds during our hydrographic survey, when surveyed serac positions are unavailable.

4. Icy Bay hydrography and sedimentation

The water properties within Icy Bay were similar during each of the three years and can be considered a two-layer system (Fig. 2a–c). Water above 10–20 m depth is cold (1–5 °C) and relatively fresh (<25 g kg^{-1}). The deeper water is warmer ($>6\,^{\circ}$C) and has a near-uniform, high salinity. Both the temperature and salinity are typical of the ACC during the months preceding our measurements (Fig. 2d and Weingartner et al., 2005). At the bottom of Icy

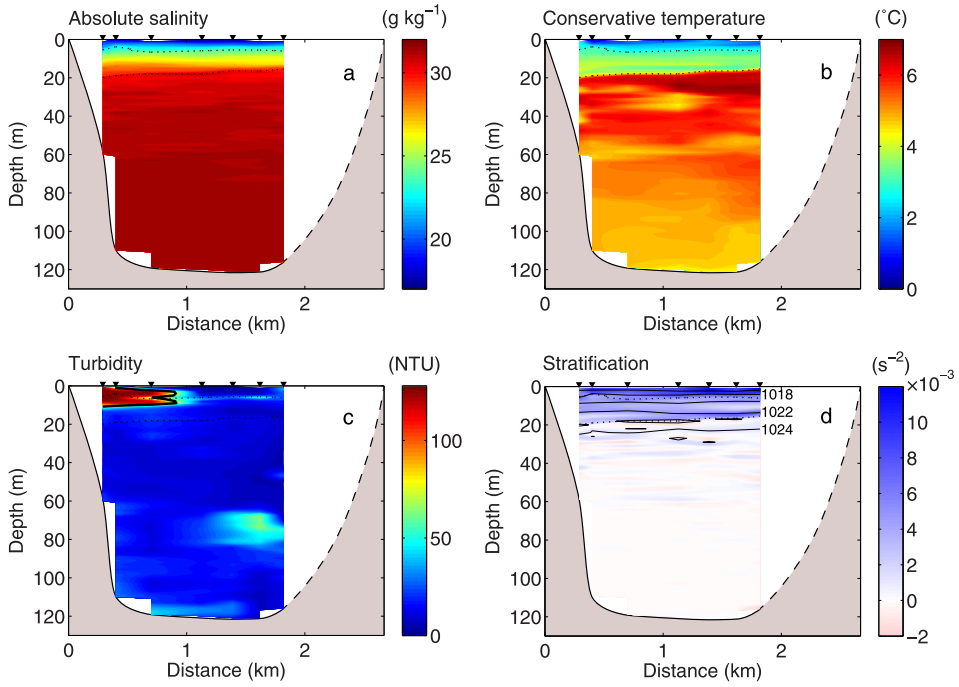

Fig. 3. Water properties in the near-terminus, fjord-perpendicular cross-section shown in Fig. 1 on 29 July 2011. View is looking up-fjord, toward Yahtse Glacier. (a) Absolute salinity, (b) conservative temperature, (c) turbidity, and (d) N^2 shown by the colorbar, overlain by black density contours (contour interval is 2 kg m^{-3}; several densities are labeled). Triangles at the top of each profile identify the locations of casts. In each panel, the 3 and 5 °C contours are dotted to aid comparison between panels. In (c), the black line highlights the 70 NTU contour, which we assume represents the bounds of the swift-flowing current out away from glacier terminus (see end of Section 6). Fjord bottom identified by CTD casts is shown, dashed where inferred. (For interpretation of the references to color in this figure, the reader is referred to the web version of this article.)

Bay, we find cool, saline water similar to the ACC during winter and spring. The warming and freshening as one moves up within the water column is consistent with the warming and freshening of the ACC through the early summer. The relatively low density of this early summer ACC water is sufficient to prevent its displacing the cooler winter water at the bottom of Icy Bay.

Vertical stratification of water within the fjord is quantified by the square of the Brunt-Väisälä frequency N,

$$N^2 = -\frac{g}{\rho}\frac{d\rho}{dz}, \tag{7}$$

where ρ is water density, g is gravitational acceleration, and z is height above sea level. Negative N^2 values indicate buoyantly unstable water volumes; increasing values of N^2 indicate increasing stability. In order to minimize small-scale instabilities, we have smoothed N^2 in all figures with a 5 m moving average. The boundary between the cold surface and warm sub-surface layer is shown in Fig. 2c by local maxima in N^2 in 2009, 2010, and 2011 at 8.8, 6.5, and 11.0 m, respectively.

Horizontal variability of water properties is far less than in the vertical; the same two layers presented within Fig. 2 can be traced throughout Icy Bay (see supplemental material). Isohalines are nearly horizontal and salinity is nearly constant at depths greater than 20 m in 2009 and 2011. Temperatures within the deep layer are 1–2 °C cooler at a given depth near the Yahtse terminus than they are 15 km farther from the terminus. At the 17 km intermediate sill, we recorded our highest water temperatures, 12 °C in 2011. We suggest that this indicates water entering upper Icy Bay from the Gulf of Alaska.

Along a line approximately 1.5 km from the terminus of Yahtse Glacier, a set of casts made on 29 July 2011 reveal water properties consistent with the broader patterns described above (Fig. 3). This profile was begun at a high tide and was completed in 2.4 h, during which time the tide fell approximately 0.8 m. Absolute salinity increases with depth from a minimum of 17 g kg^{-1} at the surface to 30 g kg^{-1} at 20 m, then increases more slowly to a uniform 31.5 g kg^{-1} at 60 m (Fig. 3a). A sharp thermocline is present between 15 and 20 m depth, below which the water temperature rises to 7 °C, then gradually decreases with depth (Fig. 3b). In 2010, when a single CTD cast was made mid-fjord at this location, we found structure similar to that shown in Fig. 2 for that year, with 10.4 °C water at 38 m depth.

The turbidity signal in 2011 is dominated by the presence of the persistent 2011 subglacial discharge plume on the northwest side of the fjord (Fig. 3c). The edge of the plume was sharp while we made our casts, with an abrupt change from blue–green water and a dense iceberg cover outside the plume to brown, rapidly flowing water free of icebergs within the plume. Water sampled within this plume exceeded the range of the turbidimeter (>128 Nephelometric Turbidity Units (NTU)). Below the plume (approximately 10 m depth) the turbidity fell quickly to background levels (∼10 NTU). Several less-pronounced lenses of turbid water were also identified, the greatest of which was between 65 and 85 m depth near the center of the fjord. This deep turbidity plume is associated with a weak, negative salinity anomaly. Dissolved oxygen and pH were highest near the surface (Supplemental Fig. S1), with the relatively high dissolved oxygen concentrations (∼6.5 mL L^{-1}) at depth suggestive of renewal at subannual timescales (Supplemental Fig. S1 and Muench and Heggie, 1978).

Stratification is high in the shallow layers where salinity changes rapidly, then falls off abruptly at the thermocline between 15 and 18 m, at approximately the 1024 kg m^{-3} isopycnal (Fig. 3f). However, smaller instabilities with $-1.5 \times 10^{-3} \lesssim N^2 \lesssim -0.5 \times 10^{-3}$ are present across the fjord down to a depth of 60–65 m. Below 65 m, the near-terminus water is less unstable, with $N^2 > -0.3 \times 10^{-3}$.

As all of the CTD casts in Fig. 3 reached the sea floor, we can compare their depths with soundings made in 1981, approximately 3 yrs after the terminus of Yahtse Glacier retreated through

this part of the fjord (Post, 1983; Porter, 1989). Thirty years prior to our casts, the fjord bottom at our cross-section was sounded between 173.4 and 181.4 m. Our casts, corrected to the same datum, are 118.9 m deep. This implies sedimentation rates ranging from 1.82 to 2.08 $m\,yr^{-1}$ at a mean distance of approximately 2.5 km from the glacier terminus. These sedimentation rates are within the ranges of previous near-glacier marine sedimentation studies within Icy Bay and elsewhere along the Gulf of Alaska coast (e.g. Cowan and Powell, 1991; Jaeger and Nittrouer, 1999; Koppes and Hallet, 2006; Goff et al., 2012).

5. Near-terminus single-cell estuarine circulation

Each of our hydrographic observations are consistent with the estuarine circulation described by Motyka et al. (2003), in which subglacial discharge emerging at depth within the fjord entrains warm seawater and, driven by its low salinity, rises buoyantly to the fjord surface. While rising, the seawater–subglacial discharge mixture flows along the submarine glacier terminus, melting ice. On the surface, the combined mixture of seawater, subglacial discharge and submarine melt comprise an outflowing plume of glacially-modified water 10–20 m thick.

The dominant circulation pattern at the head of Icy Bay appears to be shallow, glacially-modified water flowing out of the fjord over the top of ACC water. Further from the terminus, particularly over the top of the sills, more complicated circulation patterns likely prevail. These pathways are not a focus of this study. In our near-terminus section (Fig. 3), we cannot entirely rule out some component of secondary circulation, or interweaving of glacially-modified water at multiple depths (cf., Straneo et al., 2011). Water at 50–60 m depth is cooler and fresher than water above or below it. This pattern extends for approximately 15 km south from the glacier terminus. If multi-cell circulation is present, the small size of the salinity and temperature anomalies at depth (<0.4 $g\,kg^{-1}$ and $<1.2\,^{\circ}C$) indicate that it is weak. The dominance of the 10–20 m thick shallow plume and the relative homogeneity of the deeper water is consistent with the shallowness of the LIA sill and the single (ACC) origin of the seawater within Icy Bay.

The depths over which Gulf of Alaska seawater is entrained at the Yahtse Glacier terminus are unclear. However, several lines of evidence indicate that the circulation may be constrained to depths less than 60–65 m. Between 50 and 60 m, we see an abrupt $\sim 1\,^{\circ}C$ cooling. Below this depth, we see uniform, high salinities and a turbid water plume near the center of the fjord. N^2 is closer to zero, indicating a decrease in small-scale instabilities and mixing. Water near the bottom of Icy Bay may be relatively inert, and not involved in the estuarine circulation. Regardless of the details of the circulation, our across-fjord profile allows us to place bounds on the properties of the seawater entrained at the terminus by the buoyant subglacial discharge. Most likely, this entrained seawater is a mixture with properties intermediate between a deep end member ($S_A = 31.5$ $g\,kg^{-1}$, $\Theta = 4.45\,^{\circ}C$) and a shallow end member ($S_A = 30.9$ $g\,kg^{-1}$, $\Theta = 6.8\,^{\circ}C$). The mean properties over the entire near-terminus water column, appropriate for a uniform entrainment rate independent of depth, are $S_A = 30.31$ $g\,kg^{-1}$, $\Theta = 4.94\,^{\circ}C$.

6. Analysis of submarine melt rate

We consider the shallow, glacially-modified water (Fig. 3) to be a mixture from three sources: ambient seawater (with properties S_{As}, Θ_s), subglacial discharge (S_{Ad}, Θ_d), and submarine glacier melt (S_{Am}, Θ_m). Non-glacial freshwater sources were insignificant. The mouth of the only watershed >10 km^2 enters Icy Bay 18 km down-fjord of the Yahtse Glacier terminus. Rain recorded by a weather station at the Yahtse Glacier terminus during the days leading up to our CTD casts was insignificant. Furthermore, we assume that all ice melting occurs at the submarine terminus and that iceberg melt is insignificant. We are justified in this due to our close proximity to the terminus, iceberg keel depths that rarely extend below 20 m, cold near-surface water temperatures and strong stratification that inhibits mixing of warmer water up to the base of the icebergs.

On a Θ/S_A diagram (Fig. 4), any water that is purely a mixture of seawater and subglacial discharge should fall on the mixing line joining ($S_{Ad} = 0$ $g\,kg^{-1}$, $\Theta_d = 0\,^{\circ}C$) with (S_{As}, Θ_s). As there are two extreme seawater end members (a deep, cold one (a) and a shallow, warmer one (c)) both are identified with dashed mixing lines in Fig. 4. If ice is melted into a seawater–subglacial discharge mixture, the final 3-component mixture will plot below the seawater–subglacial discharge mixing line, largely as a result of the transfer of sensible seawater heat to the latent heat needed to melt ice (Gade, 1979; Jenkins, 1999). Nearly all of the water shallower than 16 m falls below the shaded region bounded by the two mixing lines; thus ice melt must be present at appreciable concentrations within this shallow, outflowing plume.

To solve for the relative mass fractions of seawater, subglacial discharge and submarine glacier melt within a given parcel of water (X_s, X_d, and X_m respectively), we simultaneously solve the following system of conservation equations

$$S_{As}X_s + S_{Ad}X_d + S_{Am}X_m = S_A \tag{8}$$

$$\Theta_s X_s + \Theta_d X_d + \Theta_m X_m = \Theta \tag{9}$$

$$X_s + X_d + X_m = 1 \tag{10}$$

where (S_A, Θ) are the measured, in-situ water properties.

Whereas $S_{Am} = 0$ $g\,kg^{-1}$, Θ_m is reduced by a variety of factors, the most significant of which is the latent heat necessary to melt ice. Thus,

$$\Theta_m = \Theta_f - \frac{L}{c_w} - \frac{c_i}{c_w}(\Theta_f - \Theta_i) \tag{11}$$

where Θ_f is the freezing point of seawater, L is the latent heat of fusion, c_w and c_i are the specific heat capacities of seawater and ice, and Θ_i is the ice temperature (Jenkins, 1999). At temperate Yahtse Glacier, where surface melt occurs during the summer even at the highest elevations, $\Theta_i = 0\,^{\circ}C$ and $\Theta_m = -83.9\,^{\circ}C$. The influence of submarine glacier melt is shown by a third mixing line in Fig. 4, which represents the potential water properties of seawater mixed with varying amounts of ice melt.

To place bounds on the mass fractions of ambient seawater, subglacial discharge and submarine melt within the near-terminus glacially-modified water, we solved Eqs. (8)–(10) at each depth and location across the fjord using the two seawater end members. These results (Fig. 5) reveal that up to 43% of the glacially-modified water is subglacial discharge. Meltwater reaches maximum concentrations between 2.3% and 4.1% of the shallowest water layers, with mean values for X_m between 0.5 and 2.8% across the glacially-modified water.

We emphasize that the water contents presented in Fig. 5 are only bounds on the true values. Neither panels (a) nor (c) of Fig. 5 are correct; a more plausible model will have values of X_d and X_m that lie between the two ends of the spectrum (Fig. 5b). For example, for the depth-averaged water properties ($S_{As} = 30.31$, $\Theta_s = 4.94\,^{\circ}C$), the mean $X_m = 1.1\%$. These results are summarized in Table 1.

In order to calculate submarine melt rates from our mass fractions, we must make an assumption about the currents within Icy Bay. Previous studies in glacierized fjords have demonstrated that instantaneous velocities, such as those measured with acoustic Doppler current profilers (ADCP), do not necessarily reflect the

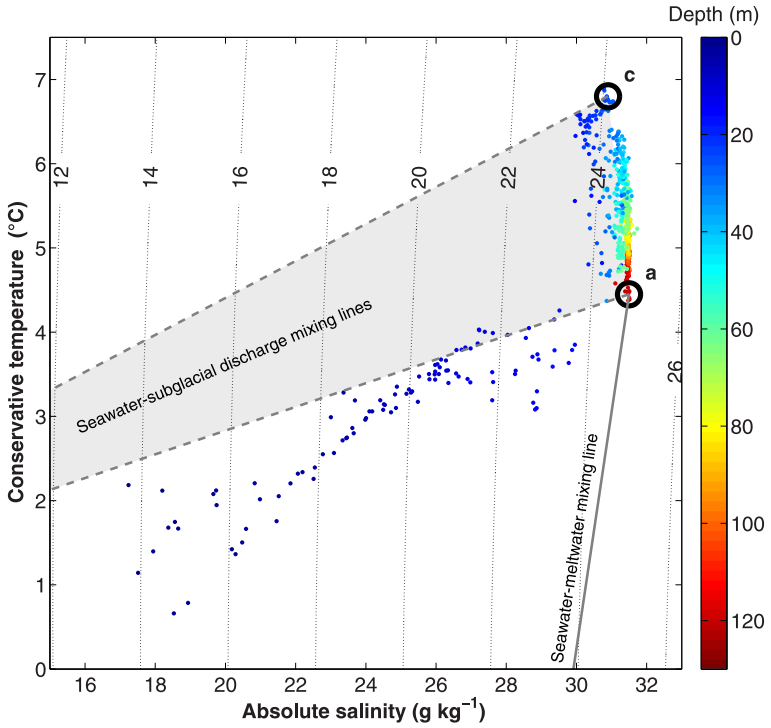

Fig. 4. Measurements of S_A and Θ at 1 m depth intervals for each of the 7 CTD casts shown in Figs. 1 and 3. Two potential seawater end members (S_{As}, Θ_s) are circled in thick black lines and labeled as (a) and (c) to match Fig. 5. Mixing lines between these end members and subglacial discharge are shown as gray dashed lines and the region between these subglacial discharge mixing lines is lightly shaded. A mixing line with ice melt (Gade, 1979; Jenkins, 1999) for the cool and deep seawater end member is shown as a solid, gray line. Meltwater lines for other Θ/S_A values have similar slopes. Finely-dotted contours of potential density anomaly ($\rho_{S_A,\Theta,0} - 1000$) are labeled in kg m^{-3}.

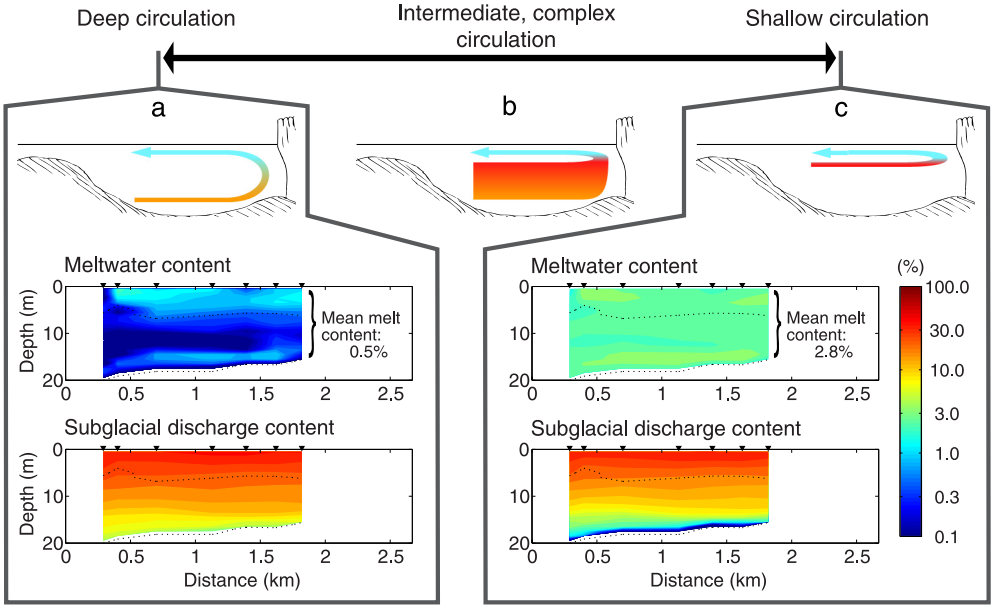

Fig. 5. The spectrum of deep to shallow possible water circulation patterns. (a) and (c) represent the extreme end members of the estuarine circulation. (b) represents a more plausible model, in that it is characterized by a more complex circulation that involves the entire fjord depth, and is bracketed between (a) and (c). Cartoons (approximately to scale, with vertical exaggeration) are longitudinal cross-sections illustrating circulation in which (a) only deep, cool seawater is entrained and melts ice at the terminus, (b) some combination of the entire water column melts ice along the terminus, and (c) only shallow, warm water is entrained and melts ice. Lower panels show the values of X_m and X_d of the glacially-modified water, calculated from the solution of Eqs. (8)–(10) for (a) $S_{As} = 31.5$ g kg^{-1}, $\Theta_s = 4.45$ °C and (c) $S_{As} = 30.9$ g kg^{-1}, $\Theta_s = 6.8$ °C. The values in (a) and (c) bound the actual water contents that result from the pattern of circulation illustrated in case (b). The locations of CTD casts and the 3 and 5 °C contours are shown as in Fig. 3.

average currents necessary to identify melt rates (Straneo et al., 2011). Instead, we draw on our time lapse photographs of the upper fjord and field observations of drift rates to estimate u_{gmw}, the mean current within the approximately 18 m-thick outflowing surface plume.

The time lapse photograph sequence reveals two distinct regions of near-surface water flow. Outside of the turbid subglacial discharge plume, icebergs drift slowly in the absence of any strong currents (left side of fjord in Fig. 6 and Supplemental Movie). In contrast, icebergs that enter the persistent subglacial discharge

Table 1
Estimates of submarine melt for three different choices of seawater (S_{As}, Θ_s) mixed through Eqs. (8)–(10). Mean X_m is the mean meltwater mass fraction in the glacially-modified water. Heat transport is the power necessary to melt Q_m. Q_d is an estimate of subglacial discharge within the glacially-modified water. Note that Q_m represents a flux of ice lost to submarine melt, whereas Q_d if a flux of water. † Comparison between u_i and $\dot{m}$ reveals that $\dot{m}$ cannot exceed 17 m d^{-1}.

Choice of (S_{As}, Θ_s)	Mean X_m (%)	Q_m (m^3 s^{-1})	Heat transport (10^9 W)	$\dot{m}$ (m d^{-1})	Q_d (m^3 s^{-1})
Warm end member	2.8	120	38	52†	650
Mean of water column	1.1	49	15	20†	650
Cold end member	0.5	20	6	9	800

Fig. 6. View south of Icy Bay, over the terminus of Yahtse Glacier, one day prior to the CTD casts that serve as the basis for this study. Image is a still frame taken from Video 1, in which the icebergs on the left (SE) 3/4 of the fjord are slowly circulating in the absence of strong near-surface currents. On the right (NW) side, the brown subglacial discharge plume with strong currents rapidly sweeps floating icebergs south into Icy Bay.

plume are quickly carried away from the glacier terminus. The turbid, brown surface of the subglacial discharge plume largely remains iceberg free. Boat drift rates at the time of our casts were consistent with this pattern. While we did record a relatively weak down-fjord drift outside of the plume, the drift rate inside the plume was far faster, exceeding 0.50 m s^{-1}. While this observation is contemporaneous with the hydrographic survey, the timelapse photographs indicate that the swift currents within the turbid plume are persistent for several months around our survey. To ensure that our assessment of submarine melt rate is conservative, we assume that a 0.50 m s^{-1} current is confined to those parts of the fjord cross-section where the turbidity was high, in excess of 70 NTU (Fig. 3c). We assume that no current exists elsewhere within the cross-section of glacially-modified water. If we average the 0.50 m s^{-1} current of the turbid water and the zero current elsewhere, $u_{\mathrm{gmw}} = 0.084$ m s^{-1}. This estimate is similar to the mean currents reported in other glacierized fjords (e.g., Motyka et al., 2003; Rignot et al., 2010; Sutherland and Straneo, 2012).

These calculations require that our currents and water properties represent tidally averaged conditions. Two lines of reasoning support this. First, tidal currents are small near the head of inlets with negligible tidal flats. A first-order, continuity-based estimate for tidal currents under these circumstances (Eq. (13) of Friedrichs and Aubrey, 1994) indicates that tidal currents during our cast profile were 0.0018 m s^{-1}. This is more than an order of magnitude smaller than u_{gmw}. Second, the flushing time for the portion of the fjord north of our casts (i.e., the fjord volume north of the profile divided by the flux of glacially-modified water) is approximately 1 day, larger than the semi-diurnal tidal timescale.

If we multiply u_{gmw} by the cross-sectional area of the glacially-modified water and its meltwater content, we arrive at meltwater fluxes for each of our choices of (S_{As}, Θ_s) in Fig. 5. We estimate that the vertical surface area of the submarine portion of the terminus is 0.21 km^2 by fitting a parabola through the maximum fjord depth. Because we assume that meltwater is sourced uniformly over the submarine terminus, we arrive at submarine melt rates between 9 and 52 m d^{-1} (Table 1). For the case of the mean salinity and temperature, $\dot{m} = 20$ m d^{-1}. However, application of Eq. (5) reveals that $\dot{m}$ should not exceed 17 m d^{-1} (next section).

7. Comparison between submarine melt rate and the near-terminus glacier velocity

Ice surface speeds near the glacier terminus derived through the calibrated image cross-correlation are 17 m d^{-1} during the July 2011 hydrographic survey (results not shown). As at other rapidly flowing, tidewater glaciers, we assume that motion between the glacier and its bed makes up the significant majority of the speed recorded at the surface (e.g., Meier et al., 1994). Furthermore the thickness (~180 m) to width (2700 m) aspect ratio of the Yahtse Glacier terminus is small. Thus we expect that lateral stress and velocity gradients will be small and the ice flow speed near the middle of the glacier is representative of the entire terminus area. While we cannot precisely quantify the depth- and width-averaged, terminus-normal glacier velocity u_i, it is most likely not significantly less than the observed rate of 17 m d^{-1}.

At Yahtse Glacier, the terminus position change dL/dt over one day is insignificant; Eq. (5) is appropriate and, on average, $\dot{c} + \dot{m} = 17$ m d^{-1}. Thus, 52 m d^{-1} of submarine melt is contradicted by observations; $\dot{c} \geqslant 0$ m d^{-1}, so $\dot{m} \lesssim 17$ m d^{-1}. Because we estimate 9 m d^{-1} as a lower bound on $\dot{m}$, the submarine melt rate is at least 50% of and may easily control the entire frontal ablation rate. Subaerial calving still occurs, but we find that it is likely paced by the rate at which submarine melt undercuts the terminus.

8. Discussion

8.1. Additional assessments of our melt rate calculation

Similar to our method of calculating the meltwater flux, we can determine the subglacial discharge Q_d by multiplying u_{gmw} by the cross-sectional area of the glacially-modified water and its subglacial discharge content. Depending on our choice of seawater source (Fig. 5), we find Q_d is between 650 and 800 m^3 s^{-1} (Table 1). We can compare this hydrographic estimate with an independent estimate of Q_d calculated from ablation over the entire 1020 km^2 surface area of Yahtse Glacier. During the 2011 melt season, the Michigan Tech Research Institute measured ablation at Bering Glacier, another highly-crevassed coastal glacier 70 km west of Yahtse Glacier. From their results, we derive an elevation-dependent ablation rate for the period immediately preceding our CTD casts. Then, by applying this ablation function to the hypsometry of Yahtse Glacier and assuming there are no changes in glacier water storage, we arrive at an ablation-based estimate for Q_d of 363 m^3 s^{-1}, approximately half the hydrographic estimate for subglacial discharge.

All of the rates presented within Table 1 scale linearly with u_{gmw}. The assumption of no change in glacier water storage is crude, but if the ablation rate Q_d estimate is correct and the hydrographic estimates for Q_d are too large by a factor of 2, then the u_{gmw} and $\dot{m}$ are also large by a factor of 2. In this case, better bounds would be $4.5 \leqslant \dot{m} \leqslant 26$. A 2-D numerical model based on Jenkins (2011) is another approach for estimating $\dot{m}$, which is entirely different than our method of un-mixing the glacially-modified water. Application of this model to our CTD casts, under

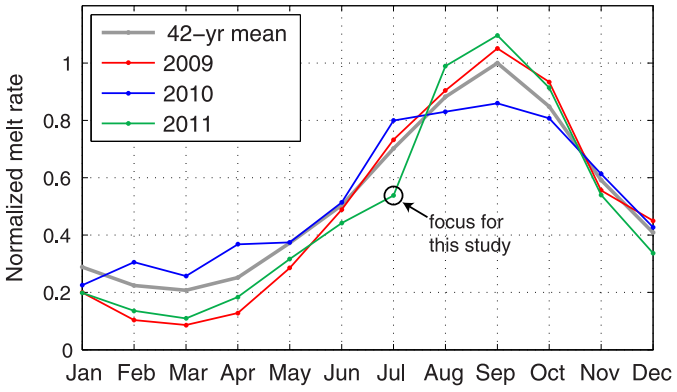

Fig. 7. Estimate of the timing of submarine melt for Gulf of Alaska tidewater glaciers. Values are calculated according to Eq. (6) with $p = 1/3$ by application of the monthly mean 20-m-depth conservative temperature from GAK1 (Royer, 2005), and the monthly mean freshwater discharge to the Gulf of Alaska (Royer, 1982). The annual cycle is not significantly different with $p = 1/2$. Melt rates are normalized by the maximum monthly rate of the 42-yr mean. The 42-yr mean uses temperature data from opportunistic casts made between 1970 and 2011; January is the least-represented month, with measurements from 14 yrs. The 2009–2011 data use the monthly mean temperature recorded by a mooring (Fig. 2d).

the assumption that subglacial discharge is released evenly across the width of the terminus, suggests that our estimate of $\dot{m}$ may be high by a factor of 2–3 (Jenkins, 2013). However, the similarity of the results from each of these approaches increases our confidence in the magnitude of our $\dot{m}$ calculation.

8.2. Seasonal to interannual context

Our late July measurements from each year are a snapshot from an annual cycle. Salinity and temperature of the ACC vary seasonally and we expect $\dot{m}$ to as well. After rising through a series of step increases, near-surface temperatures within the ACC typically reach their maximum values ($\sim$13 °C) in July and August before decaying through the fall and winter (Fig. 2d and Royer, 2005). During the summer, increases in temperature may be associated with decreases in salinity.

Relatively small-scale deviations from these seasonal patterns appear manifest within our Icy Bay casts. In 2010, the temperature of the ACC stepped from 9 to 11 °C, 18 days prior to our measurement for that year (Fig. 2d). Steps to similarly warm temperatures occurred either during or after our 2009 and 2011 measurements. In those years, temperatures prior to the casts were cooler and barely exceeded 9 °C. This interannual contrast in the ACC is reflected in the contrast among our Icy Bay CTD casts. The pronounced warmth between 20 and 60 m in 2010 demonstrates that the water reaching the heads of Icy Bay's glacierized fjords is strongly connected to the water on Alaska's continental shelf.

We can determine a first-order time series of submarine melt rates for Yahtse and other tidewater glaciers around the Gulf of Alaska by applying Eq. (6) to the ACC temperature (a proxy for Θ_s) and estimates of freshwater discharge to the Gulf of Alaska from Royer (1982) (a proxy for q). Freshwater delivery to the ACC (including contributions from subglacial discharge) peaks between September and November, with values roughly twice those typical of July. This calculation reveals that the submarine melt rate typically peaks in September, when the ACC is warm and powerful fall storms drench the Gulf of Alaska (Fig. 7). July $\dot{m}$ is typically 70% of the September maximum, however, due to the unseasonably cool July 2011 water temperatures, our calculations reveal that typical September $\dot{m}$ may be 1.8 times greater than we report in this study. In a typical year, submarine melt rates may be at least as high as we report during 6 months of the year. Again, $\dot{m} \lesssim u_i$, but these simple calculations emphasize the significance of submarine melt as a controlling mass loss process at Yahtse Glacier.

We expect that submarine melting may be an important driver of the seasonal cycle of terminus advance and retreat observed at Yahtse Glacier. The terminus is most-advanced in the spring, after the minimum in melt rate, and most-retracted in the fall, after the maximum in melt rate. Motyka et al. (2003) and Ritchie et al. (2008) report similar observations at LeConte and Hubbard Glaciers. Seasonal terminus retreat has also been reported at Columbia Glacier. There, the development of "seasonal embayments" (locally retracted regions of the terminus) were also associated with the location of turbid subglacial discharge plumes (Sikonia and Post, 1980; Krimmel and Vaughn, 1987). Sikonia and Post (1980) demonstrated a strong link between a proxy for subglacial discharge and frontal ablation rate. A seasonal embayment was present at Yahtse Glacier for much of the summer of 2011, where the terminus above the persistent, turbid plume retracted 400 m behind the rest of the terminus (Fig. 1b).

8.3. Onset of rapid tidewater glacier retreat

At their most-advanced positions, many Alaskan tidewater glaciers terminated on shallow shoals that have the potential to shield the glacier terminus from warm water at depth. The LIA maximum at Icy Bay is no deeper than 17 m; elsewhere in Alaska, sills are similarly shallow (Muench and Heggie, 1978; Walters et al., 1988). Subglacial discharge emerging at depths less than 20 m would only entrain cool water against the glacier terminus and melt rates would have been small. However, once retreat begins (perhaps through a change in climate; Post et al., 2011), ambient seawater may be exchanged with the deepening basin in front of the terminus and discharge of subglacial water at greater depths initiates the estuarine circulation described in this study and in Motyka et al. (2003). Submarine melt rates will increase.

As the terminus retreats into yet deeper water, more submarine ice surface area is exposed to warm seawater and Q_m increases, even if $\dot{m}$ remains constant. Even in $\sim$110 m deep water, the glacially-modified water that emerges at the surface of Icy Bay is several degrees above its freezing point, and thus could potentially melt more ice. Therefore, we can expect submarine melt to increase if the terminus is exposed to more warm water at depth. This mechanism offers a potential physical explanation for empirical relationships between water depth and frontal ablation rate (Brown et al., 1982; van der Veen, 2002).

8.4. Comparison with other glacier–fjord systems

Subglacial discharge and warm seawater promote submarine melt together (Eq. (6)). If the flux of subglacial discharge is the same in two different fjords, we expect submarine melt rates in the narrower fjord to be greater than those in the wider fjords. In narrow fjords, subglacial discharge is focused beneath a narrow glacier terminus (q is greater), more warm seawater is entrained (Jenkins, 2011), and a larger proportion of the glacier terminus undergoes significant submarine melt. Overall, Q_m is greater for narrow fjords, than for wide fjords. Similarly, q is also greater at glaciers with larger rates of subaerial surface melt. These glaciers should also experience larger rates of submarine melt. Thus, the submarine melt rate is linked to surface melt and runoff on the glacier surface.

In contrast, we anticipate less submarine melt where glaciers with low surface melt rates flow steeply down to tidewater within a wide fjord. This is the case at the East Greenland outlet glaciers, including Helheim and Kangerdlugssuaq Glaciers. At Helheim Glacier, mid-summer subaerial melt production is estimated at 170 $m^3\,s^{-1}$ (Andersen et al., 2010), approximately half

the melt at Yahtse Glacier, and is released at a glacier terminus that is twice as wide as that of Yahtse Glacier. Thus, it is not surprising that the submarine melt rates are small, approximately 2 $m\,d^{-1}$ (even disregarding the contrast in seawater temperature Sutherland and Straneo, 2012). Furthermore, the buoyancy flux provided by subglacial discharge is insufficient to bring all of the mixed, glacially-modified water to the surface (Straneo et al., 2011; Sciascia et al., 2013). Therefore, the fjord in front of Helheim Glacier is characterized by a more complicated circulation pattern, with glacially-modified water found at depth, as well as on the surface.

The relative warmth of the ACC compared with the east and west coasts of Greenland also plays an important part in governing submarine melt (Weingartner et al., 2005; Straneo et al., 2012). These differences in temperatures on the shelf propagate up-fjord and persist at the glacier terminus. The temperature of the ACC is at least 8 °C warmer than the water temperature at the mouths of Greenlandic fjords (Straneo et al., 2012) and at least 11 °C warmer than the water off the coast of Antarctica (Pritchard et al., 2012). These temperature contrasts can be expected to yield melt rates at Alaskan glaciers that are severalfold greater than those at either of the polar ice sheets (Eq. (6)).

Further contrasts among glacier–fjord systems, such as ice flow rate or advance/retreat state of the terminus, are unlikely to have a direct effect on the submarine melt rate. Indirect effects may come about through development of submarine moraines that can shield the terminus from the warmest water (Section 8.3), or through the generation of meltwater at the glacier bed. Faster flowing ice, with a more dynamic subglacial hydrologic system, can potentially move sediment more quickly to the terminus than slower flowing ice. If a glacier terminus is also advancing or stable, then that sediment will contribute to the development or maintenance of a submarine terminal moraine.

9. Conclusions

Near the front of Yahtse Glacier, a tidewater glacier terminating in Icy Bay, we quantified the heat deficit of the water within the cold surface layer to place bounds on the rate of submarine melt. We have demonstrated that submarine melt has the potential to match the speed at which ice flows into the terminus. Therefore, calving of subaerial icebergs may largely be a response to undercutting of the terminus during our observation period. Because approximately one third of this grounded glacier terminus is above sea level, one third of frontal ablation at Yahtse Glacier is subaerial calving. However, the rate at which subaerial calving occurs may be controlled by how quickly submarine melt removes the pedestals on which subaerial seracs rest. Process-based models that attempt to predict iceberg calving without accounting for submarine melt are unlikely to be successful.

Observations in the field are consistent with the results of this study. We observed rapid terminus retreat (the “seasonal embayment” of Section 8.2) in the vicinity of upwelling, turbid subglacial discharge, and a dearth of submarine iceberg calving events. During an early-June observation period, only 6% of visually-observed calving events involved a submarine-released iceberg despite an estimated 65% of the terminus being below sea level (Bartholomaus et al., 2012). Similar to the case at LeConte Glacier (Motyka et al., 2003), subglacial discharge produced by several $cm\,d^{-1}$ ablation over an extensive subaerial glacier surface exits through a relatively narrow glacier terminus. This drives convection at the glacier front that entrains warm, ambient seawater, melts the submarine terminus, and generates a 10–20 m-thick surface layer of water flowing out away from the glacier terminus.

We note that large, 9–17 $m\,d^{-1}$ melt rates are insufficient on their own to drive terminus retreat. Rather, the terminus of Yahtse Glacier has been advancing at 100 $m\,yr^{-1}$ for the last two decades. Similarly, most of Alaska’s tidewater glaciers are presently stable, despite the observed 0.3 °C per decade temperature increase of the ACC since the 1970s (McNabb and Hock, submitted for publication; Royer and Grosch, 2006). These observations demonstrate that other factors, such as glacier geometry, must also be important in dictating whether rapid submarine melt will be associated with terminus retreat.

Submarine melt represents an important link between the ocean and tidewater glaciers. In East Greenland, increased freshwater discharge to the coastal current enhances the rate at which cold water is advected from the north, potentially reducing submarine melt and stabilizing the tidewater glaciers found there (Murray et al., 2010). On the Alaska coast, the effect is opposite: as freshwater runoff increases, the ACC more rapidly transports warm water from lower latitudes to the mouths of Alaskas fjords (Royer, 1982; Weingartner et al., 2005). This feedback has been implicated in the ACC warming (Royer and Grosch, 2006). Should rates of freshwater delivery continue to increase (Neal et al., 2010), we can expect the strong links between the ACC and glacierized fjords to enable future increases in submarine melt rates.

Acknowledgements

This research was supported in part by a UAF Center for Global Change Student Research Grant with funds from the Cooperative Institute for Alaska Research. Additional funding was provided by the National Science Foundation through grant EAR-0810313, the USGS Climate and Land Use Change R&D program, and the Dept. of Interior Alaska Climate Science Center. This work would not have been possible without the generous loan of instruments by Roman Motyka and a skiff by Michelle Kissling; our heartiest thanks go to them. We thank Erin Pettit and Jeff Nystuen for their contributions toward collecting the CTD data from 2009. Roman Motyka, Erin Pettit, Barbara Truessel, Megan O’Sadnick, Joel Brann, Paul Aguilar, and Eric Boget assisted with field work. We thank Mark Fahnestock for providing the image cross-correlation algorithm. Comments by Johnny Sanders and three anonymous reviewers significantly improved this manuscript. We gratefully acknowledge the Institute of Marine Sciences at UAF for provision of GAK1 data (http://www.ims.uaf.edu/gak1/) and the Michigan Tech Research Institute Bering Glacier project for provision of ablation data (http://geodjango.mtri.org/gass/).

Appendix A. Supplementary material

Supplementary material related to this article can be found online at http://dx.doi.org/10.1016/j.epsl.2013.08.014.

References

Andersen, M.L., Larsen, T.B., Nettles, M., Elosegui, P., van As, D., Hamilton, G.S., Stearns, L.A., Davis, J.L., Ahlstrø m, A.P., de Juan, J., Ekström, G., Stenseng, L., Khan, S.A., Forsberg, R., Dahl-Jensen, D., 2010. Spatial and temporal melt variability at Helheim Glacier, East Greenland, and its effect on ice dynamics. J. Geophys. Res. 115, 1–18.

Arimitsu, M.L., Piatt, J.F., Madison, E.N., Conaway, J.S., Hillgruber, N., 2012. Oceanographic gradients and seabird prey community dynamics in glacial fjords. Fish. Oceanogr. 21, 148–169.

Barclay, D.J., Barclay, J.L., Calkin, P.E., Wiles, G.C., 2006. A revised and extended holocene glacial history of Icy Bay, Southern Alaska, USA. Arct. Antarct. Alp. Res. 38, 153–162.

Bartholomaus, T.C., Larsen, C.F., O’Neel, S., West, M.E., 2012. Calving seismicity from iceberg–sea surface interactions. J. Geophys. Res. 117, 1–16.

Brown, C.S., Meier, M.F., Post, A., 1982. Calving speed of Alaska tidewater glaciers, with application to Columbia Glacier. U. S. Geol. Surv. Prof. Pap. 1258-C, C1–C13.

Cogley, J.G., Hock, R., Rasmussen, L.A., Arendt, A.A., Bauder, A., Braithwaite, R.J., Jansson, P., Kaser, G., Möller, M., Nicholson, L., Zemp, M., 2011. Glossary of glacier mass balance and related terms. Technical Report. IHP-VII technical documents in hydrology No. 86, IACS Contribution No. 2. UNESCO-IHP, Paris.

Cowan, E.A., Powell, R., 1991. Ice-proximal sediment accumulation rates in a temperate glacial fjord, southeastern Alaska. In: Anderson, J.B., Ashley, G.M. (Eds.), Glacial Marine Sedimentation: Paleoclimatic Significance. In: Geol. Soc. Am. Spec. Pap., vol. 261, pp. 61–74.
Friedrichs, C.T., Aubrey, D.G., 1994. Tidal propagation in strongly convergent channels. J. Geophys. Res. 99, 3321–3336.
Gade, H.G., 1979. Melting of ice in sea water: a primitive model with application to the Antarctic ice shelf and icebergs. J. Phys. Oceanogr. 9, 189–198.
Goff, J.A., Lawson, D.E., Willems, B.A., Davis, M., Gulick, S.P.S., 2012. Morainal bank progradation and sediment accumulation in Disenchantment Bay, Alaska: Response to advancing Hubbard Glacier. J. Geophys. Res. 117, 1–15.
IOC, SCOR, IAPSO, 2010. The international thermodynamic equation of seawater – 2010: Calculation and use of thermodynamic properties. Intergovernmental Oceanographic Commission, Manuals and Guides, vol. 56. UNESCO.
Jaeger, J.M., Nittrouer, C.A., 1999. Sediment deposition in an Alaskan fjord: Controls on the formation and preservation of sedimentary structures in Icy Bay. J. Sediment. Res. 69, 1011–1026.
Jenkins, A., 1999. The impact of melting ice on ocean waters. J. Phys. Oceanogr. 29, 2370–2381.
Jenkins, A., 2011. Convection-driven melting near the grounding lines of ice shelves and tidewater glaciers. J. Phys. Oceanogr. 41, 2279–2294.
Jenkins, A., 2013. Pers. communication.
Koppes, M., Hallet, B., 2006. Erosion rates during rapid deglaciation in Icy Bay, Alaska. J. Geophys. Res. 111, 1–11.
Krimmel, R.M., Vaughn, B.H., 1987. Columbia Glacier, Alaska: changes in velocity 1977–1986. J. Geophys. Res. 92, 8961–8968.
Larsen, C.F., Motyka, R.J., Arendt, A.A., Echelmeyer, K.A., Geissler, P.E., 2007. Glacier changes in southeast Alaska and northwest British Columbia and contribution to sea level rise. J. Geophys. Res. 112, 1–11.
Matthews, J.B., 1981. The seasonal circulation of the Glacier Bay, Alaska fjord system. Estuar. Coast. Shelf Sci. 12, 679–700.
McNabb, R.W. Hock, R., submitted for publication. Alaska tidewater glacier terminus positions, 1948–2012. J. Geophys. Res.
Meier, M., Lundstrom, S., Stone, D., Kamb, B., Engelhardt, H., Humphrey, N., Dunlap, W.W., Fahnestock, M., Krimmel, R.M., Walters, R., 1994. Mechanical and hydrologic basis for the rapid motion of a large tidewater glacier. J. Geophys. Res. 99, 15219–15229.
Motyka, R.J., Hunter, L., Echelmeyer, K.A., Connor, C., 2003. Submarine melting at the terminus of a temperate tidewater glacier, LeConte Glacier, Alaska, USA. Ann. Glaciol. 36, 57–65.
Muench, R.D., Heggie, D.T., 1978. Deep water exchange in Alaskan subarctic fjords. In: Kjerfve, B. (Ed.), Estuarine Transport Processes. University of South Carolina Press, Columbia, South Carolina, pp. 239–267.
Murray, T., Scharrer, K., James, T.D., Dye, S.R., Hanna, E., Booth, A.D., Selmes, N., Luckman, A., Hughes, A.L.C., Cook, S., Huybrechts, P., 2010. Ocean regulation hypothesis for glacier dynamics in southeast Greenland and implications for ice sheet mass changes. J. Geophys. Res. 115, 1–15.
Neal, E.G., Hood, E., Smikrud, K., 2010. Contribution of glacier runoff to freshwater discharge into the Gulf of Alaska. Geophys. Res. Lett. 37, 1–5.
Nick, F.M., Vieli, A., Howat, I.M., Joughin, I., 2009. Large-scale changes in Greenland outlet glacier dynamics triggered at the terminus. Nat. Geosci. 2, 110–114.
O'Leary, M., Christoffersen, P., 2013. Calving on tidewater glaciers amplified by submarine frontal melting. Cryosphere 7, 119–128.
Porter, S.C., 1989. Late Holocene fluctuations of the fiord glacier system in Icy Bay, Alaska, USA. Arct. Antarct. Alp. Res. 21, 364.
Post, A., 1983. Preliminary bathymetry of upper Icy Bay, Alaska. U. S. Geol. Surv. Prof. Pap., OF 83-256, 1 sheet.
Post, A., O'Neel, S., Motyka, R.J., Streveler, G., 2011. A complex relationship between calving glaciers and climate. Eos Trans. AGU 92, 305.
Pritchard, H.D., Arthern, R.J., Vaughan, D.G., Edwards, L.A., 2009. Extensive dynamic thinning on the margins of the Greenland and Antarctic ice sheets. Nature 461, 971–975.
Pritchard, H.D., Ligtenberg, S.R.M., Fricker, H.a., Vaughan, D.G., van den Broeke, M.R., Padman, L., 2012. Antarctic ice-sheet loss driven by basal melting of ice shelves. Nature 484, 502–505.
Rignot, E., Koppes, M., Velicogna, I., 2010. Rapid submarine melting of the calving faces of West Greenland glaciers. Nat. Geosci. 3, 187–191.
Ritchie, J.B., Lingle, C.S., Motyka, R.J., Truffer, M., 2008. Seasonal fluctuations in the advance of a tidewater glacier and potential causes: Hubbard Glacier, Alaska, USA. J. Glaciol. 54, 401–411.
Royer, T.C., 1982. Coastal fresh water discharge in the northeast Pacific. J. Geophys. Res. 87, 2017–2021.
Royer, T.C., 2005. Hydrographic responses at a coastal site in the northern Gulf of Alaska to seasonal and interannual forcing. Deep-Sea Res., Part 2, Top. Stud. Oceanogr. 52, 267–288.
Royer, T.C., Grosch, C.E., 2006. Ocean warming and freshening in the northern Gulf of Alaska. Geophys. Res. Lett. 33, L16605.
Scambos, T.A., Dutkiewicz, M.J., Wilson, J.C., Bindschadler, R.A., 1992. Application of image cross-correlation to the measurement of glacier velocity using satellite image data. Remote Sens. Environ. 42, 177–186.
Sciascia, R., Straneo, F., Cenedese, C., Heimbach, P., 2013. Seasonal variability of submarine melt rate and circulation in an East Greenland fjord. J. Geophys. Res. 118, 1–15.
Seale, A., Christoffersen, P., Mugford, R.I., O'Leary, M., 2011. Ocean forcing of the Greenland Ice Sheet: Calving fronts and patterns of retreat identified by automatic satellite monitoring of eastern outlet glaciers. J. Geophys. Res. 116, 1–16.
Sikonia, W.G., Post, A., 1980. Columbia Glacier, Alaska; recent ice loss and its relationship to seasonal terminal embayments, thinning, and glacial flow. U.S. Geological Survey Hydrologic Investigations Atlas 619, 3.
Stabeno, P.J., Bond, N.A., Hermann, A.J., Kachel, N.B., Mordy, C.W., Overland, J.E., 2004. Meteorology and oceanography of the Northern Gulf of Alaska. Cont. Shelf Res. 24, 859–897.
Straneo, F., Curry, R.G., Sutherland, D.A., Hamilton, G.S., Cenedese, C., Våge, K., Stearns, L.A., 2011. Impact of fjord dynamics and glacial runoff on the circulation near Helheim Glacier. Nat. Geosci. 4, 322–327.
Straneo, F., Sutherland, D.A., Holland, D., Gladish, C., Hamilton, G.S., Johnson, H.L., Rignot, E., Xu, Y., Koppes, M., 2012. Characteristics of ocean waters reaching Greenland's glaciers. Ann. Glaciol. 53, 202–210.
Sutherland, D.A., Straneo, F., 2012. Estimating ocean heat transports and submarine melt rates in Sermilik Fjord, Greenland, using lowered acoustic Doppler current profiler (LADCP) velocity profiles. Ann. Glaciol. 53, 50–58.
van der Veen, C.J., 2002. Calving glaciers. Prog. Phys. Geogr. 26, 96–122.
Walters, R.A., Josberger, E.G., Driedger, C.L., 1988. Columbia Bay, Alaska: an 'upside down' estuary. Estuar. Coast. Shelf Sci. 26, 607–617.
Weingartner, T.J., Danielson, S.L., Royer, T.C., 2005. Freshwater variability and predictability in the Alaska Coastal Current. Deep-Sea Res., Part 2 52, 169–191.
Xu, Y., Rignot, E., Menemenlis, D., Koppes, M., 2012. Numerical experiments on subaqueous melting of Greenland tidewater glaciers in response to ocean warming and enhanced subglacial discharge. Ann. Glaciol. 53, 229–234.